Journal of Ceramic Processing Research. Vol. 21, No. 6, pp. 656~661 (2020)
(Received 20 May 2020, Received in revised form 2 July 2020, Accepted 16 July 2020)
https://doi.org/10.36410/jcpr.2020.21.6.656

J O U R N A L O F
Ceramic Processing Research

ZnO nanorods-based piezoelectric nanogenerators on double-sided conducting paper

G M Hasan Ul Banna[a] and Il-Kyu Park[b,*]
[a]*School of Mechanical and Electronic Engineering, East China University of Technology, Nanchang, Jiangxi, People's Republic of China*
[b]*Department of Materials Science and Engineering, Seoul National University of Science and Technology, Seoul 01811, South Korea*

We report on the voltage output enhancement from ZnO nanorod (NR)-based bendable piezoelectric nanogenerators (PENGs) with a conducting paper. Double-sided carbon paper (DSCP) was used as a conducting substrate. Structural investigations by scanning electron microscope and X-ray diffraction results showed that ZnO NRs were successfully grown via a two-step hydrothermal process on both sides of the CP. Photoluminescence peak intensity ratio of the band-edge to the deep level emissions from the ZnO NRs on both sides of the CP substrate was similar values in the range of 1.8 to 2, which indicating a similar crystalline quality of the ZnO NRs on the front and back sides. The output characteristics from the two PENG devices on the CP substrate showed identical piezoelectric output. The output voltage from the DSCP-based PENG was 2.56- and 1.86-fold greater than that from the single-sided PENG devices on only the front and back of the CP substrate, respectively. This enhancement was attributed to the synergetic effect between the PENGs on the front and back of CP and to the modification of the CP's electrical properties under an electric field generated by the PENGs on the opposite side of the CP substrate.

Keywords: ZnO, Nanorods, Nanogenerator, Hydrothermal, Piezoelectricity.

Introduction

The increasing popularity of mobile and portable devices for internet of things technologies has concentrated research focus on potential sustainable powering systems, including electrical energy scavenging from ubiquitous ambient energy such as nuclear, mechanical, thermal, and electrochemical energies. Transforming mechanical energy into electrical energy is a promising avenue anytime and anywhere because of its abundant availability in the human body and surrounding environments, such as bodily fluid movement, muscle stretching, mechanical triggering, and airflow [1-5]. There are three energy conversion techniques from mechanical sources based on triboelectric, electromagnetic, and piezoelectric principles [6]. And piezoelectric energy harvesting has attracted strong attention for energy harvesting ever since the first demonstration of a one-dimensional nanostructure-based piezoelectric nanogenerator (PENG) in 2006 and the subsequent improvements in performance for practical applications [5-14].

Among the piezoelectric materials for self-powering PENG applications, ZnO has become the most popular due to its adaptability to a wide variety of substrates, such as silicon, sapphire, metal sheet, and conducting papers for fabricating nanostructures [10-14]. In addition, it exhibits superior piezoelectric, semiconducting, nontoxic, and biodegradability properties due to its asymmetric hexagonal wurtzite structure and polar crystal structure. The development of self-powering electronic devices by using piezoelectric materials like ZnO has primarily focused on enhancing the output power of PENGs by combining various technologies, including modification of device structures or hybridization with other harvesting technologies such as solar or chemical energies [14-18]. However, recent focus has shifted to the flexibility of PENG devices in order to widen their potential applications to, for example, in-vitro sensors to monitor health conditions by a pressure sensor and paper-based diagnosis for fast and reliable detection, textile, or wearable electronics where flexibility is needed [15, 19, 20]. Therefore, current investigations are focusing on various structures and material systems, including sandwich structures, hybrid composite structures, Schottky-contact structures, and novel 2D materials [19-21]. In this paper, we report the growth of ZnO nanorods (NRs) on flexible and conductive substances. Concerning the flexibility of devices, one of conducting paper, carbon paper (CP) is a promising substrate for PENGs because of its porous structure, flexibility, and electrical conductivity [15]. Porous nature of the CP affords a large

*Corresponding author:
Tel : +82-2-970-6349
Fax: +82-2-973-6657
E-mail: pik@seoultech.ac.kr

surface area for growing higher density ZnO nanorods (NRs), which resulting in the enhancement of PENG performances. In addition, conductive CPs offers the possibility of using double-sided surface and the potential for the PENG to be hybridized with other energy conversion or storage devices, such as photovoltaics and batteries. To demonstrate these advantages, we fabricated ZnO NR-based PENGs by using the double sided carbon paper and investigated the performance of the devices.

Experimental Procedure

Fabrication

Fig. 1 shows the procedures for fabricating the PENG devices from the ZnO NRs. The ZnO NRs were grown on both surfaces of the 35 μm-thick CP substrate with a resistivity of about 10 Ω/cm^2. To grow the ZnO NRs on a single side of the CP substrate, the other side of the substrate was covered by kapton tape during the growth. For ease of description, one of the CP surfaces is defined as the front side (FS) and the other as the back side (BS). To remove all contamination, each CP substrate was cleaned with acetone, methanol, and deionized (DI) water in an ultrasonic bath for 10 min, and dried with a mild N_2 gas flow. The 0.5 cm^2 area of the right side of CP was then covered with kapton tape to prevent the growth of NRs. The seed layer of ZnO NRs and the main layer were sequentially coated on the CP substrate via a two-step hydrothermal process. In the first step, an ethanol solution with 60 mM of zinc acetate [$Zn(CH_3CO_2)_2$] was stirred at 350 rpm and heated to 100 °C and held for 10 min. The process was repeated three times to ensure uniform and complete coating of the ZnO seed layers on both sides of the porous CP surface.

In the second step, the seed layer-coated CP substrate was used to grow ZnO NRs by a hydrothermal process using a mixed solution of 60 mM zinc nitrate hexahydrate [$Zn(NO_3)_2$ $6H_2O$] and 60 mM hexamethylenetetramine [$(CH_2)_6N_4$] in DI water with stirring at 2,000 rpm and heating at 90 °C for 2 hr [15]. During the hydrothermal growth, the CP substrates were kept vertically on a sample holder in the solution, to ensure the same environment for both sides of the CP substrate. Then the samples were cleaned in DI water to completely remove free-standing ZnO crystallites from the samples by using an ultrasonic bath for 5 min. After the growth of the ZnO NRs, a 15-μm-thick polydimethylsiloxane (PDMS; Sylgard-184, Dow Corning, Midland, MI) layer was spin-coated on the ZnO NR surfaces. This PDMS prepolymer was prepared with a weight ratio of 10:1 by mixing a PDMS curing agent and a PDMS base monomer, which was coated on the ZnO NR surface by using a spin coating rotation method at 3,000 rpm for 40 sec, followed by curing at 70 °C for 30 min. These processes were repeated for both sides of the CP substrates. During this step, the possible presence of gas bubbles in the top layer can hinder the connections between ZnO NRs and PDMS layers. Therefore, the sample was evacuated in a vacuum chamber to remove the unwanted gas bubbles from the thick PDMS layers and to strengthen the penetration of the PDMS layer into both sides of the CP substrate. Ti/Au layers (5/100 nm) were deposited on both sides of the PDMS-covered ZnO NRs at room temperature (RT) by using a

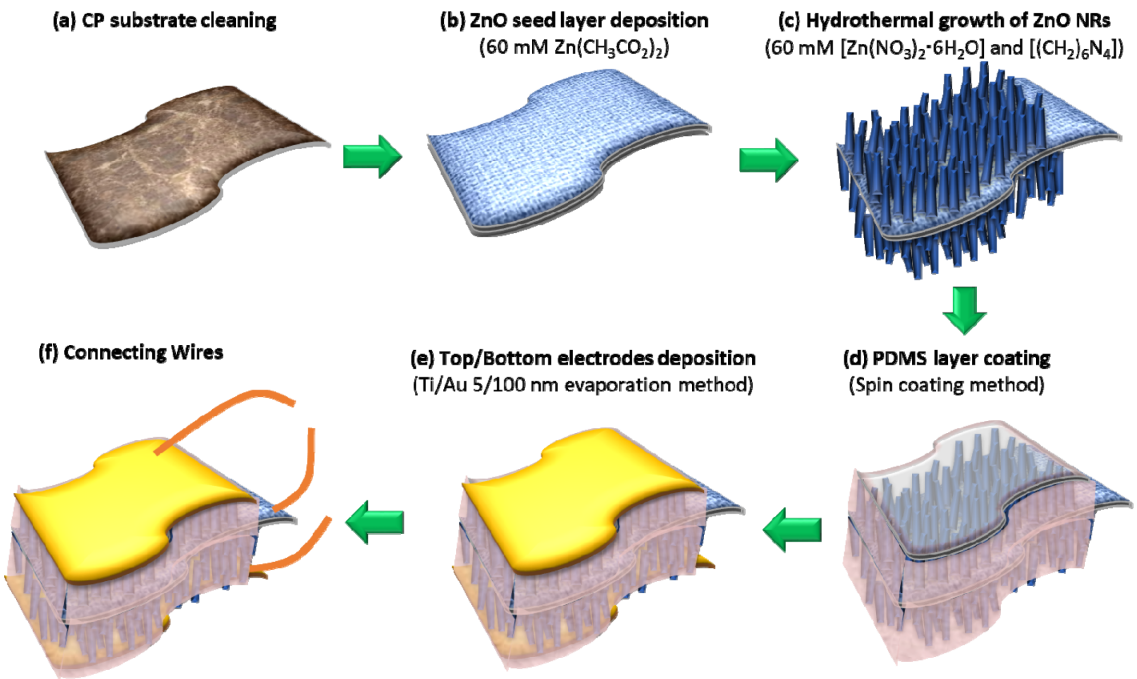

Fig. 1. Schematic of the processing steps for fabricating ZnO NR-based PENGs on DSCP.

thermal evaporator. Finally, for observing the electrical output, Cu wires were connected to the double-sided electrodes, as shown in Fig. 1(f).

Characterization

The surface topography and composition of the ZnO NRs on both sides of the CP were observed by using field-emission scanning electron microscopy (FE-SEM) and the structural properties were investigated by X-ray diffraction (XRD). The photoluminescence (PL) spectra of the ZnO NRs on both sides of the CP substrate were measured by using a continuous wave of He-Cd laser with 24 mW power and 325 nm wavelength at RT. The PENG devices were subjected to an external mechanical force by a straining system comprised of a 0.8-cm-diameter cylinder, in which the device surface was hit repeatedly and a periodic mechanical compressive stress was applied. In this continuous stress-and-relax process, the output voltages were measured simultaneously by using an oscilloscope (TBS1202B, Tektronix).

Results and Discussion

Fig. 2 shows FE-SEM images of the ZnO NRs deposited on the front and back of CP with a molar concentration of 75 mM. The ZnO NRs on the porous surface of CP were grown in random directions and showed a similar shape on both sides. However, the density of the ZnO NRs was slightly higher on the back of CP compared to that on the front. The surface of the ZnO NRs showed a hexagonal columnar structure. This implies that each ZnO NR was a wurtzite-structured single crystal that was grown along the *c*-direction.

Fig. 3 shows the XRD results that reveal the crystal structure of the ZnO NRs on both sides of the CP substrate. The broad peak at around 26.5° is attributed to the short-range order of the amorphous phase of the CP substrate. The sharp diffraction peaks correspond to the (100), (002), (101), (102), and (110) planes of hexagonal wurtzite structure of ZnO (space group: P63mc; a = 0.32501 nm, c = 0.52071 nm). The diffraction data were in agreement with the JCPDS card for ZnO (JCPDS 79-2205). There were no diffraction peaks except those for the CP substrate and ZnO. This indicates that no secondary phase or impurity was detected. The substrate peaks of the ZnO NRs on the FS of the CP have greater intensity than those of the BS, which confirms the better crystallinity of the NRs in the BS.

Fig. 4(a) shows the PL spectra of the ZnO NRs grown on both sides of the porous CP substrate at RT. A sharp peak at 380 nm and a relatively weak peak at 520 nm were observed in both FS and BS spectra. The sharp peak in the ultraviolet range corresponds to the band-edge emission of ZnO NRs. The broad emission band in the visible spectral range is due to the deep level emissions from the ZnO NRs, which originate from various impurities in the ZnO crystal, such as oxygen deficiency due to electron recombination, zinc interstitials, and their complexes [22, 23]. These point defects usually act as a donor to generate free charge carriers. The generated free charge carriers in the ZnO NRs are detrimentally affected by screening the generated

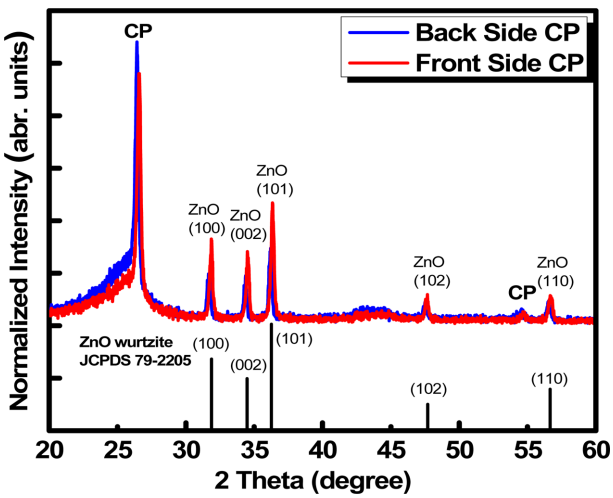

Fig. 3. XRD patterns of ZnO NRs on DSCP.

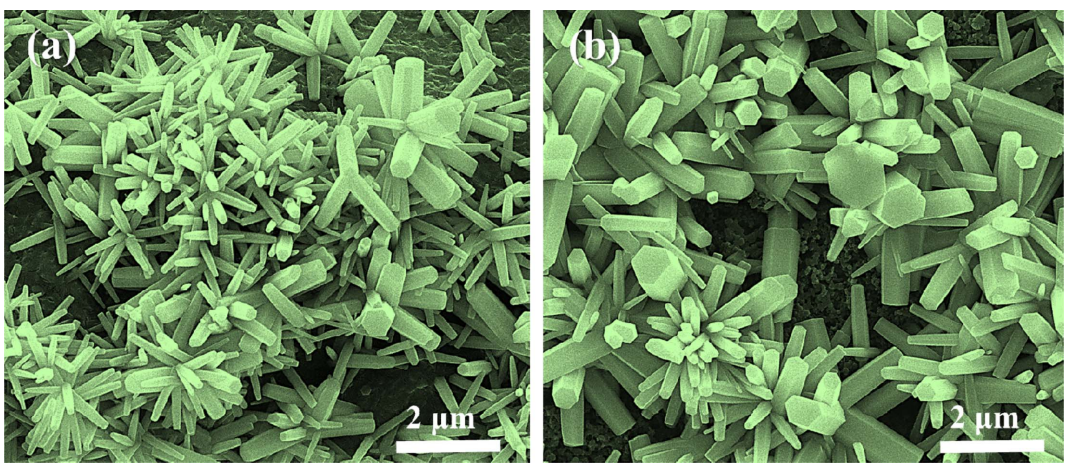

Fig. 2. FE-SEM images of the ZnO NRs on DSCP: (a) FS and (b) BS.

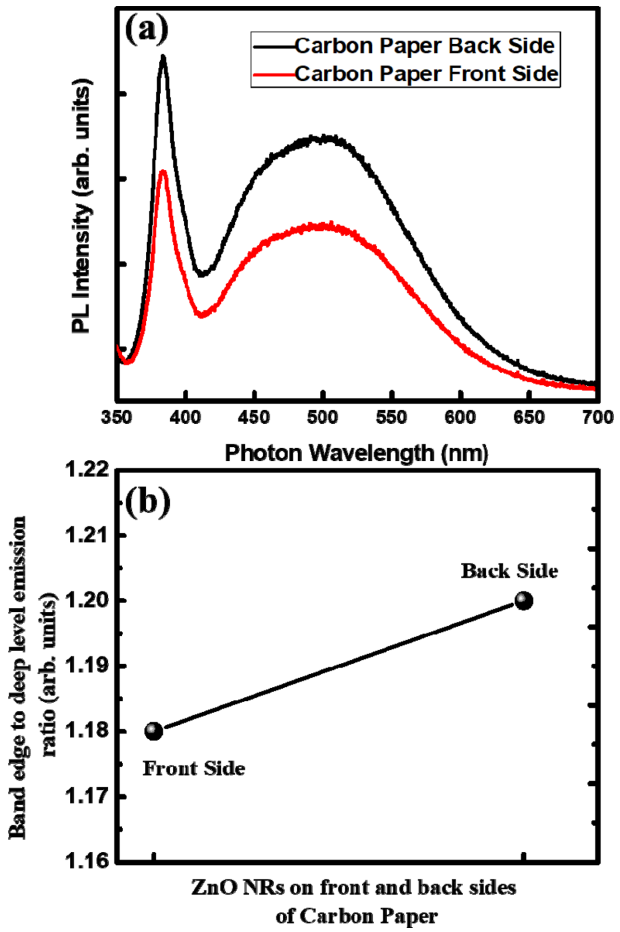

Fig. 4. (a) Comparison of PL spectra for the front and back of carbon paper measured at RT for ZnO NRs on DSCP. (b) The band-edge emission to deep level emission ratio for the ZnO NRs grown on the front and back of DSCP.

piezoelectric potential on the output voltage performance of the designed PENG devices [7, 24, 25]. Therefore, the crystalline quality of the ZnO NRs on each side of the CP substrate was investigated by comparing the intensity of the deep level emission. Fig. 4(b) shows the PL peak intensity ratio of the band-edge to the deep level emissions from the ZnO NRs on both sides of the CP substrate. The intensity ratios of 1.18 and 1.20 on the FS and BS, respectively, imply that the ZnO NRs' crystalline quality was slightly better on the BS than on the FS. This result agrees with the morphological results that show the vividly uniform and denser growth of ZnO NRs on the back as shown in Fig. 2(b). This is attributed to the inevitable difference in the amounts of Zn and O supplied to both sides of the substrate during the hydrothermal growth.

Fig. 5 shows the voltage outputs of the PENG devices fabricated on the DSCP substrate with the same strain frequency at 2.2 Hz. For simplicity, we denoted PENGs on the front only, back only, and double sided as PENG-F, PENG-B, and PENG-D, respectively. When stress is applied to and released from the PENGs, despite the variation in output voltage on each side, all

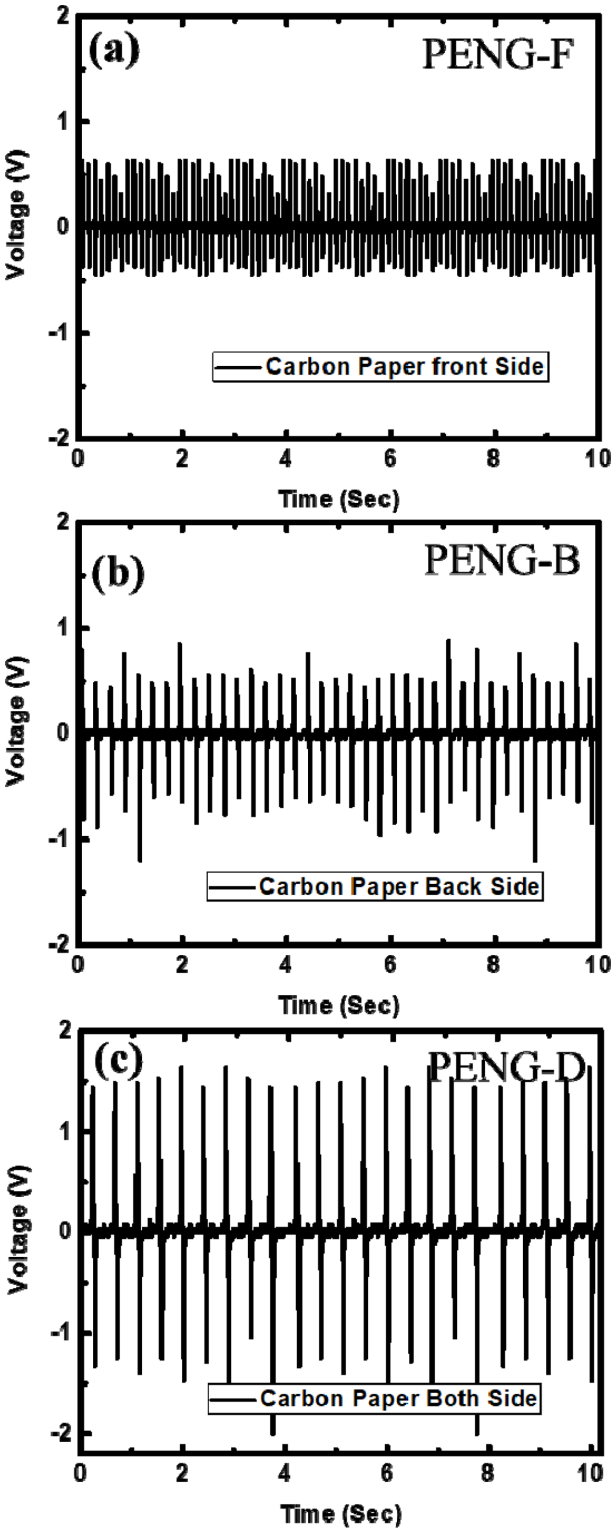

Fig. 5. Output voltage from ZnO NRs-based PENGs on carbon paper: (a) PENG-F, (b) PENG-B, and (c) PENG-D under a strain frequency of 2.2 Hz.

three PENGs showed positive and negative peaks due to the charging and discharging, respectively. This is attributed to the alternating current (AC) signals produced by the stress along the perpendicular direction to the vertically aligned ZnO NRs in the PENG device. The

figure shows that the output voltage remains an AC signal while the ZnO NRs are grown in random direction, which is attributed to the elastomeric property of the PDMS polymer layer which helps the transfer of the applied strain to both the whole PENG device and the individual ZnO NRs. The Young's modulus of the PDMS polymer ranges between 0.57 and 3.7 MPa [26], while that of the ZnO NRs is about 29 GPa [27]. Therefore, the Young's modulus is about four orders of magnitude larger for the ZnO NRs than that for the PDMS layer. As a result, when the stress is applied to the PENG device, the PDMS layer is deformed first and the stress is distributed to the individual ZnO NRs equally [28]. Therefore, the PDMS layer plays a critical role in transferring the applied stress in this PENG device in the isotropic directions to the ZnO NRs.

PENG-B generated a larger output voltage (0.88V) than PENG-F (0.64 V) due to the denser ZnO NRs, as shown in Fig. 2, and exhibited better crystallinity, as shown in Fig. 3. The free charge carriers that were generated by impurities in the ZnO NRs detrimentally affected the PENG performance by screening the generated piezoelectric potential [8, 29]. The voltage output of PENG-D (1.64 V) was enhanced about 2.56 and 1.86-fold compared to that of PENG-F and PENG-B, respectively. The enhanced voltage output would attributed to the electric field-induced synergetic effect between the front and back of the CP substrate and the modification of the CP substrate resistance under the electric field generated by the PENGs. And this enhancement mechanism can be explained as follows. Fig. 6 shows the operating principle and enhancement mechanism of the PENG device on the CP substrates. A negative potential is initially created at the top of the ZnO NRs when stress is applied to only one side of the PENG device, and is then delivered to the electrodes through the PDMS layers, thus generating a negative pulse. As the stress is subsequently removed, the piezoelectric potential suddenly vanishes, which allows the stored charge in the electrode to return through the external circuit and generate a positive pulse, as occurs in other ZnO NR-based PENG devices. The operation principle of PENG-D can be regarded as a combination of two devices. The piezoelectric potential generated as the ZnO NR experiences an external tensile or compression stress on the surface causes relative displacement of Zn^{2+} cations with respect to O^{2-} anions. The amount of maximum piezoelectric potential generated from a single ZnO NR under external mechanical stress for vertical (F_V) and lateral (F_L) directions can be expressed as $V_{max} = |F_V|\gamma_V(L/\pi R^2)$ and $V_{max} = |F_L|\gamma_L(1/\pi R)$, respectively [7,10,28], where γ_V and γ_L denote the piezoelectric voltage parameters in vertical and lateral directions of ZnO NRs, respectively, and R and L denote the radius and length of each ZnO NR, respectively. These equations imply that if the NR's radius and length are unchanged then the piezoelectric output from each ZnO NR is always constant and is directly proportional to the maximum deflection of the individual NR. Therefore, as the number of ZnO NRs in the PENG devices increases, greater piezoelectric potential is generated because each ZnO NR can act as an individual voltage source. This is consistent with the results that the output voltages from PENG-D are

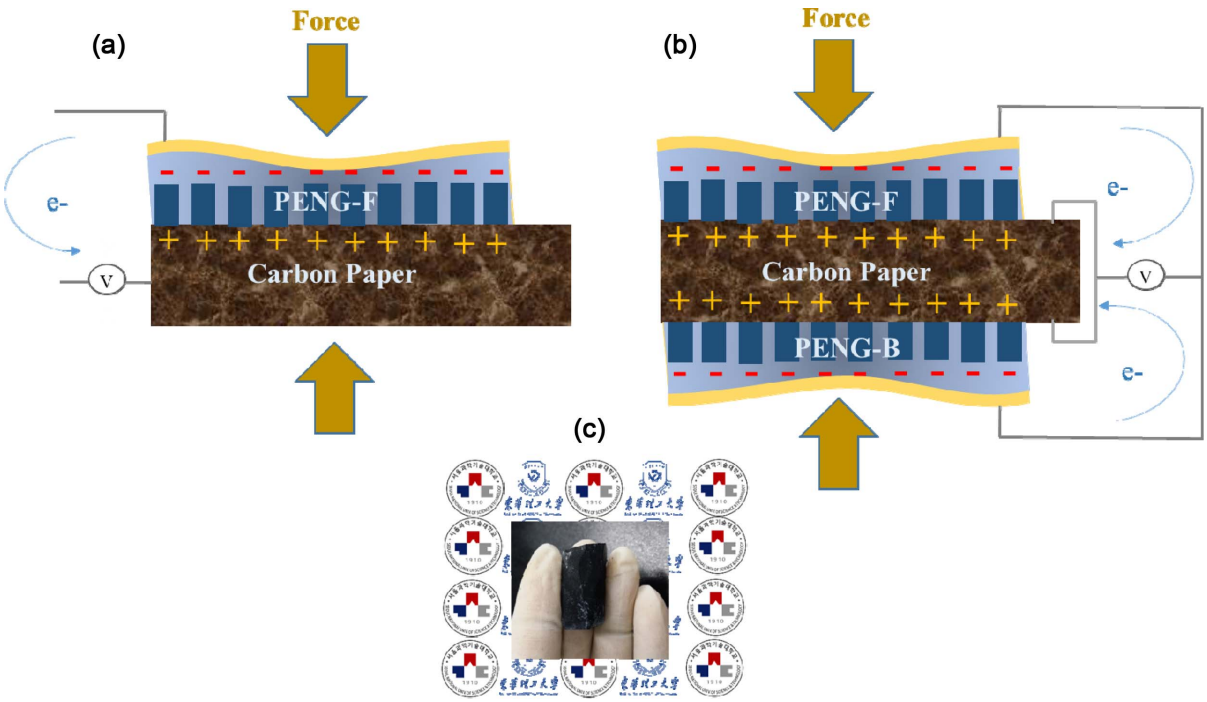

Fig. 6. Schematic of PENG device structure on (a) single side (either front or back) and (b) DSCP substrates operating under compressive stress. (c) Bendability of the PENG device on DSCP.

enhanced by 2.56 and 1.86-fold compared to that of PENG-F and PENG-B, respectively. In PENG-D, the electrons of both sides sequentially enforce and then reinforce the flow from the PENG device where the electric field is generated. This enables more electrons to flow through the external circuit and accumulate together and finally be measured by using the connected measurement systems. An electric field-induced synergetic effect between PENG-F and PENG-B enhanced the PENG-D output, which was 1.08-fold greater than the sum of the individual voltage outputs of PENG-F and PENG-B. This explains the enhanced output voltage performance from PENG-D compared to that of the two single-sided PENG devices. This enhancement is further attributed to the modification of the electrical properties under a generated electric field. Due to the electron scattering mechanism, the resistance of the substrate can be modified under an electric field [30]. Therefore, PENG-D can enhance the output voltage. In addition, the flexibility of the fabricated device, as shown in Fig. 6(c), will allow its use in bendable applications such as for in-vitro medical sensors and textile devices.

Conclusions

In summary, we have fabricated ZnO NR-based PENGs exhibiting enhanced output voltage by using a DSCP substrate. Morphological investigation showed that the ZnO NRs were grown in the similar shape and length on both sides of the CP surface, but with a slightly larger density on the back. The XRD and PL results confirmed that the crystal quality of the ZnO NRs on both sides of the substrate exhibited similar degree. The voltage output from PENG-D was 2.56- and 1.86-fold greater than those from PENG-F and PENG-B, respectively. The enhanced voltage output is attributed to the electric field-induced synergetic effect between the front and back of the CP substrate and the modified electrical resistance of the CP substrate under the electric field generated by the operating PENGs. These results demonstrate the capability of the ZnO NR-based PENG on the DSCP to enhance their output voltage as well as the possible application to bendable self-powering devices.

Acknowledgments

This study was supported by the Research program funded by the Seoultech (Seoul National University of Science & Technology).

References

1. Z.L. Wang and J. Song, Science 312 (2006) 242-246.
2. Z.L. Wang, Sci. Am. 298 (2008) 82-87.
3. Y. Hu, Y. Zhang, C. Xu, L. Lin, R.L. Snyder, and Z.L. Wang, Nano Lett. 11 (2011) 2572-2577.
4. Z.L. Wang and W. Wu, Angew. Chem. Int. Ed. 51 (2012) 11700-11721.
5. K.K. Kim and I.K. Park, J. Ceram. Process. Res. 18 (2017) 435-439.
6. S. Beeby, M. Tudor, and N. White, Meas. Sci. Technol. (2006) R175.
7. J. Sohn, S. Cha, B. Song, S. Lee, S. Kim, J. Ku, H. Kim, Y. Park, B. Choi, Z L. Wang, J.M. Kim, and K. Kim, Energy Environ. Sci. (2013) 97-104.
8. M.Y. Choi, D. Choi, M.J. Jin, I. Kim, S.H. Kim, J.Y. Choi, S.Y. Lee, J.M. Kim, and S.W. Kim, Adv. Mater. 21 (2009) 2185-2189.
9. H.K. Park, K.Y. Lee, J.S. Seo, J.A. Jeong, H.K. Kim, D. Choi, and S.W. Kim, Adv. Funct. Mater. 21 (2011) 1187-1193.
10. Y. Gao and Z.L. Wang, Nano Lett. 7 (2007) 2499-2505.
11. D.Y. Lee, H. Kim, H.M. Li, A.R. Jang, Y.D. Lim, S.N. Cha, Y.J. Park, D.J. Kang, and W.J. Yoo, Nanotechnology 24 (2013).
12. D.Y. Jung, S.H. Baek, M.R. Hasan, and I.K. Park, J. Alloy Compd. 641 (2015) 163-169.
13. G.H. Nam, S.H. Baek, C.H. Cho, and I.K. Park, Nanoscale 6 (2014) 11653-11658.
14. M.R. Hasan, S.H. Baek, K.S. Seong, J.H. Kim, and I.K. Park, ACS Appl. Mater. Inter. 7 (2015) 5768-5774.
15. G.M.H.U. Banna and I.K. Park, Nanotechnology 28 (2017) 445402.
16. S.H. Baek, M.R. Hasan, and I.K. Park, Nanotechnology 27 (2016) 065401.
17. C. Xu and Z.L. Wang, Adv. Mater. 23 (2011) 873-877.
18. C. Liu, A. Yu, M. Peng, M. Song, W. Liu, Y. Zhang, and J. Zhai, J. Phys. Chem. C 120 (2016) 6971-6977.
19. K. Y. Lee, J. Chun, J.H. Lee, K.N. Kim, N.R. Kang, J.Y. Kim, M.H. Kim, K.S. Shin, M.K. Gupta, J.M. Baik, and S.W. Kim, Adv. Mater. 26 (2014) 5037-5042.
20. K.I. Park, C.K. Jeong, J. Ryu, G.T. Hwang, and K.J. Lee, Adv. Energy Mater. 3 (2013) 1539-1544.
21. G. Zhu, R. Yang, S. Wang, and Z.L. Wang, Nano Lett. 10 (2010) 3151-3155.
22. L.E. Greene, M. Law, J. Goldberger, F. Kim, J.C. Johnson, Y. Zhang, R.J. Saykally, and P. Yang, Angew. Chem. Int. Ed. 42 (2003) 3031-3034.
23. A.C. Arsenault, T.J. Clark, G. Von Freymann, L. Cademartiri, R. Sapienza, J. Bertolotti, E. Vekris, S. Wong, V. Kitaev, I. Manners, R. Z. Wang, S. John, D. Wiersma, and G.A. Ozin, Nat. Mater. 5 (2006) 179-184.
24. D. Li, Y.H. Leung, A.B. Djurišić, Z.T. Liu, M.H. Xie, S.L. Shi, S.J. Xu, and W.K. Chan, Appl. Phys. Lett. 85 (2004) 1601-1603.
25. R. Yang, Y. Qin, L. Dai, and Z.L. Wang, Nat. Nanotech. 4 (2009) 34-39.
26. J. Song, X. Wang, E. Riedo, and Z.L. Wang, Nano Lett. 5 (2005) 1954-1958.
27. X. Li, Y. Chen, A. Kumar, A. Mahmoud, J.A. Nychka, and H.J. Chung, ACS Appl. Mater. Inter. 7 (2015) 20753-20760.
28. G. Romano, G. Mantini, A. Di Carlo, A. D'Amico, C. Falconi, and Z.L. Wang, Nanotechnology 22 (2011) 465401.
29. D. Kim, K.Y. Lee, M.K. Gupta, S. Majumder, and S.W. Kim, Adv. Funct. Mater. 24 (2014) 6949-6955.
30. E. Ahilea and A.A. Hirsch, J. Appl. Phys. 42 (1971) 5601-5608.